Title	Biogeographic variation in skull morphology across the Kra Isthmus in dusky leaf monkeys
Author(s)	Ito, Tsuyoshi; Koyabu, Daisuke
Citation	Journal of Zoological Systematics and Evolutionary Research (2018), 56(4): 599-610
Issue Date	2018-11
URL	http://hdl.handle.net/2433/243819
Right	This is the peer reviewed version of the following article: [Tsuyoshi Ito, Daisuke Koyabu. Biogeographic variation in skull morphology across the Kra Isthmus in dusky leaf monkeys. 'Journal of Zoological Systematics and Evolutionary Research' 56(4), 599-610], which has been published in final form at https://doi.org/10.1111/jzs.12229. This article may be used for non-commercial purposes in accordance with Wiley Terms and Conditions for Use of Self-Archived Versions.; The full-text file will be made open to the public on 04 October 2019 in accordance with publisher's 'Terms and Conditions for Self-Archiving'; This is not the published version. Please cite only the published version. この論文は出版社版でありません。引用の際には出版社版をご確認ご利用ください。
Type	Journal Article
Textversion	author

Biogeographic variation in skull morphology across the Kra Isthmus in dusky leaf monkeys

Running title: Biogeographic variation in dusky leaf monkeys

Tsuyoshi Ito[1], Daisuke Koyabu[2]

[1]Department of Evolution and Phylogeny, Primate Research Institute, Kyoto University, Inuyama, Aichi 484-8506, Japan

[2]The University Museum, The University of Tokyo, Hongo 7-3-1, Bunkyo-ku, Tokyo 113-0033, Japan

Corresponding author: Tsuyoshi Ito

E-mail: ito.tsuyoshi.3a@kyoto-u.ac.jp

Keywords: geometric morphometrics; Southeast Asia; Thai–Malay Peninsula

1

Abstract

Despite the growing literature on the underlying factors of geographical phenotypic variation, little is known about how and to what extent biogeographical barriers in Southeast Asia have shaped morphological variation in primates. We aimed to investigate the geographical variations in skull morphology in dusky leaf monkeys by decomposing them into clinal (latitudinal), non-clinal spatial (discrete difference between regions north and south of the Isthmus of Kra), and environment-related components. We applied geometric morphometrics to measure 53 adult male specimens from 36 localities, covering the regions both north and south of the Isthmus of Kra. A linear model was used to test the effects of region (north vs. south of the Isthmus of Kra), latitude, and environmental factors (temperature and rainfall) on the size and shape of skulls. A part of variation in skull shape differed moderately between the regions in the north and south of the Isthmus of Kra, and this difference cannot be explained by latitudinal and environmental factors. However, for size and the majority of variations in shape, we detected limited contributions of region and the two environmental factors. Shape differentiation that was unexplained by latitudinal and environmental factors suggests that dusky leaf monkeys may have experienced a population division due to habitat constriction around the Isthmus of Kra. However, this divergence probably has been obscured by subsequent gene flow between populations after habitat recovery.

Introduction

Understanding the processes underlying biogeographic phenotypic diversity is one of the major challenges in evolutionary biology. In particular, non-human primates have been intensively investigated as a model to understand the biogeographical patterns and diversification history of humans. To date, spatial distributions of size and other aspects of phenotype have been well described (e.g., Fooden & Albrecht 1999; Frost, Marcus, Bookstein, Reddy, & Delson 2003; Hamada, Watanabe, & Iwamoto 1996; Rae, Hill, Hamada, & Koppe 2003). With recent advances in the worldwide climatic database and biogeographic statistics, it has been increasingly recognized that both spatial and environmental factors (e.g., temperature and rainfall) are significant predictors of morphological variations among primates (e.g., Caceres et al. 2014; Cardini, Jansson, & Elton 2007; Dunn, Cardini, & Elton 2013). However, such recent studies have mostly targeted continental patterns. Little is known about how primate morphology varies biogeographically in Southeast Asia, an area composed of numerous peninsulas/islands and that is undoubtedly influenced by sea-level fluctuations.

The Isthmus of Kra (IOK; the narrowest part of the Thai–Malay peninsula, at approximately 10 ºN) has been recognized as one of the key biogeographic boundaries for various taxa in Southeast Asia. Arguably, the IOK forms the boundary between the Sundaic and Indochinese biotas (Wallace 1876). It has long been believed that the Neogene seaways surrounding the IOK accounted for the formation of floral and faunal transitions in this region (Haq, Hardenbol, & Vail 1987; Hughes, Round, & Woodruff 2003; Woodruff 2003). However, recent paleoenvironmental studies have proposed that Neogene rises in sea level were not sufficient to bisect the Thai–Malay peninsula (Lisiecki & Raymo 2005; Miller et al. 2005; Naish & Wilson 2009). Accumulating biogeographic evidence supports this proposition and further suggests that the rise in the Neogene sea level caused the compression

of the faunal population along the Thai peninsula; this compression, along with climatic zone transition, was responsible for the faunal transition (Hannah 2009; Hughes, Satasook, Bates, Bumrungsri, & Jones 2011; Parnell 2013; Woodruff & Turner 2009). Thus, the faunal transition in this region may have been historically formed by non-geophysical (i.e., ecological and climatic) factors, making the IOK distinct among known biogeographical boundaries.

Some species or pairs of closely related species of terrestrial vertebrates are distributed cross-boundary, and despite the absence of geophysical barriers, they are often considerably differentiated both genetically and morphologically between the regions north and south of the Thai–Malay peninsula (e.g., de Bruyn, Nugroho, Hossain, Wilson, & Mather 2005; den Tex & Leonard 2013; Endo, Hayashida, & Fukuta 2007; Endo et al. 2000b; Hamada, Suryobroto, Goto, & Malaivijitnond 2008; Hayashida et al. 2007; Luo et al. 2004; Tosi, Morales, & Melnick 2002). Other taxa, however, show more complex biogeographical patterns. For example, southern populations show polymorphisms while northern ones do not [e.g., pelage color in stump-tailed macaques (Koyabu, Malaivijitnond, & Hamada 2008), and skull morphology and cytotypes in tree shrews (Endo et al. 2000a; Hirai et al. 2002)]. In contrast, studies on long-tailed macaques with dense regional sampling have revealed that body size and relative tail length vary gradually along the peninsula, with no obvious discontinuous transition at the IOK (Fooden 2006; Fooden & Albrecht 1999), following the patterns predicted by Bergmann's and Allen's rules. Other dense regional samplings have also shown that even when clear genetic and/or morphological subdivisions are observed, the transitional zone is not necessarily consistent with the IOK in various taxa (Bunlungsup, Imai, Hamada, Matsudaira, & Malaivijitnond 2017; Dejtaradol et al. 2016; Malaivijitnond et al. 2012; Patou et al. 2010). These findings suggest that although organisms were geographically isolated and differentiated between northern and southern regions at some

point in the past, they could have been admixed and homogenized via gene flow, through developmental, and/or adaptive responses to current climatic gradient across the IOK, at least for these taxa.

Morphological evidence can provide important clues for biogeographical inferences by taking advantage of vast museum collections that enable dense regional sampling (McLean et al. 2016). However, the vestige of ancient population subdivisions, if any, can be obscured by recent gene flow and/or responses to current environmental conditions, which makes morphological data ambiguous in the case of attempts to interpret phylogeographical history. One solution to this dilemma is to statistically decompose morphological variations in order to reveal the concealed vestige. For example, statistically decomposing skull morphological variations into size and shape components and then testing the biogeographical patterns of each component has been demonstrated to be an effective approach (e.g., Cardini & Elton 2009; Elton, Dunn, & Cardini 2010; Frost et al. 2003). In theory, this is because skull shape is less liable to change than is its size, and it is therefore likely to represent the historical background rather than the current environment (Cardini & Elton 2009). Further dissecting each morphological component into spatial and environment-related variations will aid interpretation of the phylogeographic history of a taxon (Cardini & Elton 2009; Cardini et al. 2007).

The present study examines the geographic variations in skull morphology in dusky leaf monkeys (*Trachypithecus obscurus*, Reid 1837), which are distributed widely and across the IOK on the Thai–Malay peninsula (Figure 1; Brandon-Jones et al. 2004; Groves 2001). Considering the paleobiogeographical history of the IOK, we hypothesize that dusky leaf monkeys were divided into northern and southern populations due to habitat constriction during the Neogene. Such a geographical isolation, if any, should have caused morphological differentiation between the northern and southern populations; however, after land recovery,

such differences may have been obscured by subsequent gene flow, developmental, and/or adaptive responses to current climatic gradients. We tested this hypothesis by decomposing craniometric variations into size and shape components and evaluating the influence of three key factors (clinal, non-clinal, and environmental factors) on each component. If discrete differences are detected between the northern and southern populations, and if these differences can be explained neither by clinal (latitudinal) nor environmental factors, the most probable scenario would be that the ancient geographical barrier around the IOK has prevented gene flow and driven differentiation. In contrast, the absence of such discrete differences would likely indicate that the two populations had not been divided into regions north and south of the IOK or that they were completely admixed and homogenized after re-connection; however, the two may be difficult to distinguish. Detection of the mosaics of discrete and clinal variations independent of environmental factors would indicate a higher probability of the isolation and re-connection scenario.

Materials and methods

The sample comprised 53 adult male specimens of dusky leaf monkeys from 36 localities (Appendix 1, Figure 1). Maturity was judged by full eruption of molars. Specimens showing any pathological signs were excluded from this study. The specimens are currently housed at the Natural History Museum (London, UK), the National Museum of Natural History (Washington DC, USA), and the Lee Kong Chian Natural History Museum (Singapore).

Sixty-seven 3D landmarks were acquired from the skulls using a Microscribe 3DX digitizer (Appendix 2) by a single observer. The cranium and mandible were occluded and firmly fused together by Pritt MULTI-FIX Haftpunkte clay (Henkel, Düsseldorf). Missing landmarks on one side were estimated by mirroring those on the other side. Missing

landmarks on midsagittal or bilaterally-missing ones were estimated by mapping weighted averages from the complete dataset onto the missing specimen using the “Morpho” package (Schlager 2017) in R statistical software (R Core Team 2017). After filling in missing landmarks, generalized Procrustes analysis was performed to superimpose landmark configurations using MorphoJ software (Klingenberg 2011). Centroid size was calculated as the square root of the sum of squares of the distances of all landmarks from the centroid. The natural logarithm of centroid size was used for size variable. Symmetrical shape components were subjected to principal component (PC) analysis to summarize skull shape variations in MorphoJ.

To partition the skull variation into clinal, non-clinal spatial, and environmental components, multivariate linear regressions were conducted using “car” package (Fox & Weisberg 2011) in R. Size or shape, represented by each PC score, was separately used as the response variable. Explanatory variables consisted of size (if response variable is PC score), region, latitude, and two environmental variables, as follows. Region was defined as the dummy variable, wherein the localities north of the IOK were coded as “0” and those south of it as “1.” Latitude was used to evaluate clinal spatial variation, because the distribution of the dusty monkey populations stretches from the north to the south of the Thai–Malay peninsula. Environmental variables consisted of annual mean temperature and annual precipitation for the past 30 years (1970–2000), and were obtained from the WorldClim database using the “raster” package (Robert 2016) in R (Figure 1). A stepwise Akaike information criterion (AIC) was conducted to identify the best model (i.e., the best combination of explanatory variables that appropriately predict a response variable) using the “MuMIn” package (Kamil 2016) in R. If region was selected as an explanatory variable, the relative level of support of each model was evaluated by the change in AIC (ΔAIC). Models with ΔAIC values of 0–2 provided substantial support, whereas ΔAIC > 4 indicated

considerably lower support compared with the best model (Burnham & Anderson 2003).

We also evaluated the Procrustes coordinate data as it is (in place of PC scores), because individual PC axes are not necessarily biologically meaningful. The symmetric shape components were regressed onto the same set of explanatory variables using "geomorph" package (Adams & Otárola‐Castillo 2013) in R. Residual randomization permutation procedure was utilized for the test of significance (Collyer, Sekora, & Adams 2015). Finally, to evaluate phenetic relationships among individuals, a neighbor-joining tree (Saitou & Nei 1987) was constructed based on the Procrustes distance matrix of the symmetric shape components as well as the residuals from the regression of them on size (allometry-adjusted symmetric shape components). For this, the "shapes" (Dryden 2017) and "ape" packages (Paradis, Claude, & Strimmer 2004) in R were used.

Prior to performing statistical analyses, outliers were detected based on Smirnov-Grubbs test ($P < 0.05$) and removed (three outliers were detected in the two environmental variables, and an additional 0–2 outliers in the PCs). The data used in this study is available at Dryad (doi:10.5061/dryad.1989g0t).

Results

The first 8 PCs accounted for more than half of the total variance in the model (Table 1), and their distance matrix was highly correlated with Procrustes distance matrix of symmetric shape components ($r \geq 0.90$). Size was not influenced by latitude, region, or annual mean temperature, whereas it was larger in localities with higher annual precipitation. Most major shape variables (PCs) were also independent of latitude or simply exhibited latitudinal cline without significant differentiation between the regions north and south of the IOK. For example, PC1 was slightly, but not significantly, explained only by annual mean temperature. PC2 and PC6 scores gradually increased or decreased with increasing latitude,

and no gap was observed at the IOK (Table 1; Figure 2). Only for PC4 was the model greatly improved by incorporating region as an explanatory variable (Appendix 3), wherein PC4 scores were significantly smaller in the northern than in the southern region of the IOK. This indicated that the face was relatively shorter, the anterior portion of the mandible was more robust, and the inferior margin of the mandible was wider in the region north of the IOK than in the south (Figure 3). PC8 scores were larger in the north than were expected by a latitudinal cline, but this effect was tentative, as indicated by ΔAIC (Appendix 3; Figure 2). For the test using the Procrustes coordinate data as response variable, regional difference was detected, but this difference disappeared in the full model that takes into account for the effects of latitudinal and two environmental factors (Table 2). A neighbor-joining phenogram also did not show clear clusters of northern and southern populations (Figure 4).

Discussion

The present study tested the hypothesis that the vestige of population subdivision is preserved in shape components, which are hidden under major variations in environment-sensitive morphological characters. For this purpose, we first decomposed skull variations into size and shape components, and then assessed the relative contributions of the ancient biogeographical barrier at the IOK and other factors to each of their variations.

Size was not significantly correlated with latitude, region (north vs. south of the IOK), nor annual mean temperature. However, it was significantly larger in the localities with higher annual precipitation. Whereas mammals in temperate or cold environments often show latitudinal size cline or negative correlation with temperature as predicted by Bergmann's rule (Ito, Nishimura, & Takai 2014), it is known that size variation is more highly correlated to annual precipitation than to temperature in the tropics (Capellini & Gosling 2007; Cardini et al. 2007; Dunbar 1990). Such size variation in the tropics is considered to

be a consequence of a response to the primary productivity of plants, and hence food availability, which is largely influenced by rainfall (Cardini, Dunn, O'Higgins, & Elton 2013). The present finding in dusky leaf monkeys is congruent with these previous findings. On the other hand, most shape components were virtually independent from the environmental factors examined (annual mean temperature and annual precipitation) or simply showed a latitudinal cline with no gap at the IOK. This indicates that observed variations in skull shape do not reflect responses to current environmental conditions nor ancient genetic isolations. Alternatively, they likely reflect gene flow among populations and/or other unknown factors. The star-shaped phenogram (Figure 3) and no significant regional difference in the test of Procrustes coordinate data also supports the regional homogeneity of this species. A part of shape variation (only PC4) was differentiated between the regions south and north of the IOK. As this discrete difference was not explained by latitudinal or environmental factors, this could be a result of ancient genetic isolation. Since this region likely had no geophysical barrier in the Neogene or later (Lisiecki & Raymo 2005; Miller et al. 2005; Naish & Wilson 2009), it seems that the rise in sea level may have caused a habitat compression around the IOK, and thus genetic isolation between northern and southern populations (see Woodruff & Turner 2009). Thus, there might have been ancient genetic isolation influencing on the north-south differentiation in the skulls of dusky leaf monkeys, but the differences probably have been much blurred by subsequent substantial gene flow after the recovery of habitat connection.

For organisms capable of relatively wide dispersals, diverged lineages can be easily admixed, and genetic pools are often homogenized across the IOK (see Bunlungsup et al. 2017; Osada et al. 2010). As with the skull shape of dusky leaf monkeys, the pelage color variations found in stump-tailed macaques also suggest such a history of isolation and re-connection (Koyabu et al. 2008). In contrast, in some primate taxa from the Malay Peninsula,

populations North and South of the IOK are even assigned into species-level differences. For example, pig-tailed macaques are divided into two species, and the boundary between the two is assumed to be located around the Surat Thani–Krabi depression, which is just south of the IOK (Malaivijitnond et al. 2012). The northern and southern species of pig-tailed macaques are dissimilar on a number of morphological characters such as facial length and sexual swelling patterns (Gippoliti 2001). The Bengal slow loris, which is distributed north of the IOK, is considerably different from its southern relative, that is the Sunda slow loris, in skull morphology and peleage color (Nekaris & Jaffe 2007; Nekaris, Blackham, & Nijman 2008; Ravosa 1998). Such a heterogeneity in the degree of admixture and morphological differentiations among taxa would be of great research interest, and may be caused by the differences in responsiveness to fluctuating habitat compressions. In conclusion, we add dusky leaf monkeys as another example of likely having experienced an ancient genetic isolation followed by substantial gene flow, although the impact and role of the IOK in shaping biogeographic variations in Southeast Asia is still disputed. Future studies are expected to elucidate the mechanisms of the maintenance of morphological differences in some specific taxa as well as the consequences of genetic admixture around the IOK.

Acknowledgements

We thank Mikiko Tanaka for her help with data preparation. We thank Kelvin Lim of Lee Kong Chian Natural History Museum for his kind care during the observations. We also thank Elisabeth Haring and anonymous reviewers for their constructive comments that greatly improved this paper. This study was funded by the Keihanshin Consortium for Fostering the Next Generation of Global Leaders in Research (K-CONNEX) (to T.I.) and JSPS Grants-in-Aid for Scientific Research (Grant 17K15195 to T.I. and 26711023 to D.K.).

References

Adams, D. C. & Otárola-Castillo, E. (2013). Geomorph: An R package for the collection and analysis of geometric morphometric shape data. *Methods in Ecology and Evolution*, **4**, 393-399.

Brandon-Jones, D., Eudey, A. A., Geissmann, T., Groves, C. P., Melnick, D. J., Morales, J. C., Shekelle, M., & Stewart, C. B. (2004). Asian primate classification. *International Journal of Primatology*, **25**, 97-164.

Bunlungsup, S., Imai, H., Hamada, Y., Matsudaira, K., & Malaivijitnond, S. (2017). Mitochondrial DNA and two Y-chromosome genes of common long-tailed macaques (*Macaca fascicularis fascicularis*) throughout Thailand and vicinity. *American Journal of Primatology*, **79**, e22596

Burnham, K. P. & Anderson, D. R. (2003). *Model selection and multimodel inference: a practical information-theoretic approach*. New York: Springer.

Caceres, N., Meloro, C., Carotenuto, F., Passaro, F., Sponchiado, J., Melo, G. L., & Raia, P. (2014). Ecogeographical variation in skull shape of capuchin monkeys. *Journal of Biogeography*, **41**, 501-512.

Capellini, I. & Gosling, L. M. (2007). Habitat primary production and the evolution of body size within the hartebeest clade. *Biological Journal of the Linnean Society*, **92**, 431-440.

Cardini, A., Dunn, J., O'Higgins, P., & Elton, S. (2013). Clines in Africa: does size vary in the same way among widespread sub-Saharan monkeys? *Journal of Biogeography*, **40**, 370-381.

Cardini, A. & Elton, S. (2009). Geographical and taxonomic influences on cranial variation in red colobus monkeys (Primates, Colobinae): introducing a new approach to 'morph' monkeys. *Global Ecology and Biogeography*, **18**, 243-263.

267 Cardini, A., Jansson, A.-U., & Elton, S. (2007). A geometric morphometric approach to the
268 study of ecogeographical and clinical variation in vervet monkeys. *Journal of*
269 *Biogeography*, **34**, 1663-1678.

270 Collyer, M. L., Sekora, D. J., & Adams, D. C. (2015). A method for analysis of phenotypic
271 change for phenotypes described by high-dimensional data. *Heredity*, **115**, 357-365.

272 de Bruyn, M., Nugroho, E., Hossain, M. M., Wilson, J. C., & Mather, P. B. (2005).
273 Phylogeographic evidence for the existence of an ancient biogeographic barrier: the
274 Isthmus of Kra Seaway. *Heredity*, **94**, 370-378.

275 Dejtaradol, A., Renner, S. C., Karapan, S., Bates, P. J. J., Moyle, R. G., & Päckert, M. (2016).
276 Indochinese-Sundaic faunal transition and phylogeographical divides north of the Isthmus
277 of Kra in Southeast Asian Bulbuls (Aves: Pycnonotidae). *Journal of Biogeography*, **43**,
278 471-483.

279 den Tex, R. J. & Leonard, J. A. (2013). A molecular phylogeny of Asian barbets: speciation
280 and extinction in the tropics. *Molecular Phylogenetics and Evolution*, **68**, 1-13.

281 Dryden, I. L. (2017). *shapes: Statistical Shape Analysis*. R package version 1.2.0. Retrieved
282 from https://cran.r-project.org/web/packages/shapes/index.html

283 Dunbar, R. I. M. (1990). Environmental determinants of intraspecific variation in body-weight
284 in baboons (*Papio* spp). *Journal of Zoology*, **220**, 157-169.

285 Dunn, J., Cardini, A., & Elton, S. (2013). Biogeographic variation in the baboon: dissecting the
286 cline. *Journal of Anatomy*, **223**, 337-352.

287 Elton, S., Dunn, J., & Cardini, A. (2010). Size variation facilitates population divergence but
288 does not explain it all: an example study from a widespread African monkey. *Biological*
289 *Journal of the Linnean Society*, **101**, 823-843.

290 Endo, H., Hayashi, Y., Rerkamnuaychoke, W., Nadee, N., Nabhitabhata, J., Kawamoto, Y.,

Hirai, H., Kimura, J., Nishida, T., & Yamada, J. (2000a). Sympatric distribution of the two morphological types of the common tree shrew in Hat-Yai Districts (South Thailand). *Journal of Veterinary Medical Science*, **62**, 759-761.

Endo, H., Hayashida, A., & Fukuta, K. (2007). Multivariate analyses of the skull size and shape in the five geographical populations of the lesser false vampire. *Mammal Study*, **32**, 23-31.

Endo, H., Nishiumi, I., Hayashi, Y., Rashdi, A. B. M., Nadee, N., Nabhitabhata, J., Kawamoto, Y., Kimura, J., Nishida, T., & Yamada, J. (2000b). Multivariate analysis in skull osteometry of the common tree shrew from both sides of the Isthmus of Kra in southern Thailand. *Journal of Veterinary Medical Science*, **62**, 375-378.

Fooden, J. (2006). Comparative review of *fascicularis*-group species of macaques (Primates: *Macaca*). *Fieldiana Zoology*, **107**, 1-44.

Fooden, J. & Albrecht, G. H. (1999). Tail-length evolution in *fascicularis*-group macaques (Cercopithecidae: *Macaca*). *International Journal of Primatology*, **20**, 431-440.

Fox, J. & Weisberg, S. (2011). *An R Companion to Applied Regression.* (Second edn.). Thousand Oaks CA: Sage.

Frost, S. R., Marcus, L. F., Bookstein, F. L., Reddy, D. P., & Delson, E. (2003). Cranial allometry, phylogeography, and systematics of large-bodied papionins (primates: Cercopithecinae) inferred from geometric morphometric analysis of landmark data. *The Anatomical Record Part A: Discoveries in Molecular, Cellular, and Evolutionary Biology*, **275A**, 1048-1072.

Gippoliti, S. (2001). Notes on the taxonomy of *Macaca nemestrina leonina* Blyth, 1863 (Primates: Cercopithecidae). *Hystrix, the Italian Journal of Mammalogy*, **12**, 51-54.

Groves, C. P. (2001). *Primate taxonomy*. Washington DC: Smithonian Institution Press.

315 Hamada, Y., Suryobroto, B., Goto, S., & Malaivijitnond, S. (2008). Morphological and body
316 color variation in Thai *Macaca fascicularis fascicularis* north and south of the Isthmus of
317 Kra. *International Journal of Primatology*, **29**, 1271-1294.

318 Hamada, Y., Watanabe, T., & Iwamoto, M. (1996). Morphological variations among local
319 populations of Japanese macaque (*Macaca fuscata*). In T. Shotake & K. Wada (Eds.),
320 *Variations in the Asian macaques* (pp. 97-115). Tokyo: Tokyo University Press.

321 Hannah, L. (2009). New insights on a classic topic: The biogeography of Southeast-Asian
322 mammals. *Frontiers of Biogeography*, **1**, 8-10.

323 Haq, B. U., Hardenbol, J., & Vail, P. R. (1987). Chronology of fluctuating sea levels since the
324 Triassic. *Science*, **235**, 1156-1167.

325 Hayashida, A., Endo, H., Sasaki, M., Oshida, T., Kimura, J., Waengsothorn, S., Kitamura, N.,
326 & Yamada, J. (2007). Geographical variation in skull morphology of gray-bellied squirrel
327 Callosciurus caniceps. *Journal of Veterinary Medical Science*, **69**, 149-157.

328 Hirai, H., Hirai, Y., Kawamoto, Y., Endo, H., Kimura, J., & Rerkamnuaychoke, W. (2002).
329 Cytogenetic differentiation of two sympatric tree shrew taxa found in the southern part of
330 the Isthmus of Kra. *Chromosome Research*, **10**, 313-327.

331 Hughes, A. C., Satasook, C., Bates, P. J., Bumrungsri, S., & Jones, G. (2011). Explaining the
332 causes of the zoogeographic transition around the Isthmus of Kra: using bats as a case
333 study. *Journal of Biogeography*, **38**, 2362-2372.

334 Hughes, J. B., Round, P. D., & Woodruff, D. S. (2003). The Indochinese–Sundaic faunal
335 transition at the Isthmus of Kra: an analysis of resident forest bird species distributions.
336 *Journal of Biogeography*, **30**, 569-580.

337 Ito, T., Nishimura, T., & Takai, M. (2014). Ecogeographical and phylogenetic effects on
338 craniofacial variation in macaques. *American Journal of Physical Anthropology*, **154**, 27-

339 41.

340 Kamil, B. (2016). *MuMIn: Multi-Model Inference*. R package version 1.15.6. Retrieved from
341 https://cran.r-project.org/web/packages/MuMIn/index.html

342 Klingenberg, C. R. (2011). MorphoJ: an integrated software package for geometric
343 morphometrics. *Molecular Ecology Resources*, **11**, 353-357.

344 Koyabu, D. B., Malaivijitnond, S., & Hamada, Y. (2008). Pelage color variation of *Macaca*
345 *arctoides* and its evolutionary implications. *International Journal of Primatology*, **29**,
346 531-541.

347 Lisiecki, L. E. & Raymo, M. E. (2005). A Pliocene-Pleistocene stack of 57 globally distributed
348 benthic δ18O records. *Paleoceanography*, **20**, PA1003.

349 Luo, S.-J., Kim, J.-H., Johnson, W. E., Van Der Walt, J., Martenson, J., Yuhki, N., Miquelle, D.
350 G., Uphyrkina, O., Goodrich, J. M., & Quigley, H. B. (2004). Phylogeography and genetic
351 ancestry of tigers (*Panthera tigris*). *PLoS Biology*, **2**, e442.

352 Malaivijitnond, S., Arsaithamkul, V., Tanaka, H., Pomchote, P., Jaroenporn, S., Suryobroto, B.,
353 & Hamada, Y. (2012). Boundary zone between northern and southern pig-tailed macaques
354 and their morphological differences. *Primates*, **53**, 377-389.

355 McLean, B. S., Bell, K. C., Dunnum, J. L., Abrahamson, B., Colella, J. P., Deardorff, E. R.,
356 Weber, J. A., Jones, A. K., Salazar-Miralles, F., & Cook, J. A. (2016). Natural history
357 collections-based research: progress, promise, and best practices. *Journal of Mammalogy*,
358 **97**, 287-297.

359 Miller, K. G., Kominz, M. A., Browning, J. V., Wright, J. D., Mountain, G. S., Katz, M. E.,
360 Sugarman, P. J., Cramer, B. S., Christie-Blick, N., & Pekar, S. F. (2005). The Phanerozoic
361 record of global sea-level change. *Science*, **310**, 1293-1298.

362 Naish, T. R. & Wilson, G. S. (2009). Constraints on the amplitude of Mid-Pliocene (3.6-2.4Ma)

363 eustatic sea-level fluctuations from the New Zealand shallow-marine sediment record.
364 *Philosophical Transactions of the Royal Society A: Mathematical, Physical and*
365 *Engineering Sciences*, **367**, 169-187.

366 Nekaris, K. & Jaffe, S. (2007). Unexpected diversity of slow lorises (*Nycticebus* spp.) within
367 the Javan pet trade implications for slow loris taxonomy. *Contributions to Zoology*, **76**.

368 Nekaris, K. A. I., Blackham, G. V., & Nijman, V. (2008). Conservation implications of low
369 encounter rates of five nocturnal primate species (*Nycticebus* spp.) in Asia. *Biodiversity*
370 *and Conservation*, **17**, 733-747.

371 Osada, N., Uno, Y., Mineta, K., Kameoka, Y., Takahashi, I., & Terao, K. (2010). Ancient
372 genome-wide admixture extends beyond the current hybrid zone between *Macaca*
373 *fascicularis* and *M. mulatta*. *Molecular Ecology*, **19**, 2884-2895.

374 Paradis, E., Claude, J., & Strimmer, K. (2004). APE: analyses of phylogenetics and evolution
375 in R language. *Bioinformatics*, **20**, 289-290.

376 Parnell, J. (2013). The biogeography of the Isthmus of Kra region: a review. *Nordic Journal of*
377 *Botany*, **31**, 001-015.

378 Patou, M.-L., Wilting, A., Gaubert, P., Esselstyn, J. A., Cruaud, C., Jennings, A. P., Fickel, J.,
379 & Veron, G. (2010). Evolutionary history of the *Paradoxurus* palm civets - a new model
380 for Asian biogeography. *Journal of Biogeography*, **37**, 2077-2097.

381 R Core Team (2017). *R: A language and environment for statistical computing*. R foundation
382 for Statistical Computing, Vienna.

383 Rae, T. C., Hill, R. A., Hamada, Y., & Koppe, T. (2003). Clinical variation of sinus volume in
384 Japanese macaques (*Macaca fuscata*). *American Journal of Primatology*, **59**, 153-158.

385 Ravosa, M. J. (1998). Cranial allometry and geographic variation in slow lorises (*Nycticebus*).
386 *American Journal of Primatology*, **45**, 225-243.

Robert, J. H. (2016). *raster: Geographic Data Analysis and Modeling*. R package version 2.5-8. Retrieved from https://cran.r-project.org/web/packages/raster/index.html

Saitou, N. & Nei, M. (1987). The neighbor-joining method: a new method for reconstructing phylogenetic trees. *Molecular Biology and Evolution*, **4**, 406-425.

Schlager, S. (2017). Morpho and Rvcg - Shape Analysis in R. In G. Zheng, S. Li, & G. Szekely (Eds.), *Statistical Shape and Deformation Analysis: Methods, Implementation and Applications* (pp. 217-256). San Diego: Academic Press.

Tosi, A. J., Morales, J. C., & Melnick, D. J. (2002). Y-chromosome and mitochondrial markers in *Macaca fascicularis* indicate introgression with Indochinese *M. mulatta* and a biogeographic barrier in the isthmus of Kra. *International Journal of Primatology,* **23**, 161-178.

Wallace, A. R. (1876). *The geographical distribution of animals: with a study of the relations of living and extinct faunas as elucidating the past changes of the earth's surface*. London: Macmillan.

Woodruff, D. S. (2003). Neogene marine transgressions, palaeogeography and biogeographic transitions on the Thai–Malay Peninsula. *Journal of Biogeography,* **30**, 551-567.

Woodruff, D. S. & Turner, L. M. (2009). The Indochinese-Sundaic zoogeographic transition: a description and analysis of terrestrial mammal species distributions. *Journal of Biogeography*, **36**, 803-821.

Figure legends

Figure 1. Thirty-six localities of skull samples (black circles). Map is color-coded by **(a)** the distribution of *Trachypithecus obscurus* (red mesh; the IUCN Red List of Threatened Species, version 2016-3); **(b)** annual mean temperature (ºC × 10); and **(c)** annual precipitation (mm).

Figure 2. Biogeographic variations in skull shape as indicated by principal components (PCs). **(a)** PC2; solid line indicates OLS regression line for total samples. **(b)** PC4; solid and dashed lines indicate median, and first and third quartiles, respectively, which are calculated separately for regions north and south of the IOK. **(c)** PC6; solid line indicates OLS regression line for total samples. **(d)** PC8; dotted line indicates OLS regression line for localities south of the IOK. Open circles indicate individuals originating from south of the IOK, and gray-filled ones indicate those from the north.

Figure 3. Shape changes along principal component (PC) axes: **(a)** PC2; **(b)** PC4; **(c)** PC6; and **(d)** PC8. Wireframes and points indicate dorsal (left) and lateral (right) views of skulls. Thin lines and open circles denote mean shape, while dark lines and filled circles denote positive extreme along each PC axis (+3 standard deviations).

Figure 4. Neighbor-joining phenogram based on Procrustes distances of skull shape: (a) the raw symmetric shape component; (b) the residuals from the regression of symmetric component on size. Open circles indicate individuals originating from south of the IOK, and gray-filled ones indicate those from the north.

428 **Tables**

429

Table 1. Summary of PCA and the best model.

	% variance	Cumulative %	Intercept	Size			Latitude			Region (south vs. north of IOK)			Annual mean temperature			Annual precipitation		
			β	β	% exp.	P	β	% exp.	P	β	% exp.	P	β	% exp.	P	β	% exp.	P
Size			0.016													0.36	9.1	0.033
PC1	13.1	13.1	-0.002										-0.34	4.7	0.129			
PC2	9.0	22.2	0.002	0.28	8.8	0.028	-0.32	10.7	0.016									
PC3	7.9	30.1	0.115	0.19	3.8	0.168							-0.34	4.6	0.129			
PC4	6.7	36.7	0.120							0.34	16.3	0.004						
PC5	5.8	42.6	0.005	0.31	9.9	0.026												
PC6	5.4	47.9	0.050				0.33	9.5	0.027				-0.35	4.9	0.106			
PC7	4.8	52.7	0.021															
PC8	4.0	56.7	0.016	-0.24	6.0	0.083	-0.54	10.8	0.022	-0.54	10.8	0.022						

β, standardized partial regression coefficient; % exp., the percentage of which a response variable is explained by an explanatory variable (based on Type II ANOVA).

The total number of tests we performed are 14 (size and PC1-13); the results of PC9-13 are not shown. When Bonferroni adjusted, no effects are significant, but the effect of region on PC4 is close to significance (P = 0.056).

430

431

Table 2. Results of Procrustes regression of skull shape.

	Df	SS (×100)	MS (×100)	R^2	F	Z	P
			Full model				
Size	1	0.50	0.50	0.03	1.54	2.15	0.014
Latitude	1	0.33	0.33	0.02	1.02	0.59	0.284
Region (south vs. north of IOK)	1	0.34	0.34	0.02	1.06	0.76	0.232
Annual mean temperature	1	0.38	0.38	0.02	1.15	1.06	0.138
Annual precipitation	1	0.20	0.20	0.01	0.61	-1.29	0.900
Residuals	44	14.35	0.33				
Total	49	16.32					
			Size and region				
Size	1	0.51	0.51	0.03	1.57	2.01	0.023
Region (south vs. north of IOK)	1	0.54	0.54	0.03	1.67	2.17	0.015
Residuals	47	15.26	0.32				
Total	49	16.32					

434

Appendices

Appendix 1. Specimens used in this study.

ID	Storage†	Locality	Remarks
104444	NMNH	Malaysia (no detailed info)	
112709	NMNH	2'18"N 103'17""E, Johor, Malaysia	
115497	NMNH	2'50"N 103'14"E, Rompin River, Pahang, Malaysia	
115498	NMNH	2'50"N 103'14"E, Rompin River, Pahang, Malaysia	
124113	NMNH	12'40"N 98'56"E, Tanintharyi, Burma	
124177	NMNH	12'40"N 98'56"E, Tanintharyi, Burma	
14.12.8.27	NHM	10'09"N, 98'36"E, Bankachon, S Tenasserim, Burma	
14.12.8.27a	NHM	10'09"N, 98'36"E, Bankachon, S Tenasserim, Burma	
14.12.8.27b	NHM	12'07"N, 99'03"E, Banlaw, Great Tenasserim river, Burma	
14.12.8.27c	NHM	8'12"N, 99'43"E, Khao Wang, Peninsular Siam	
1980.161	NHM	12'30"N, 98'22"E, King Island, Mergui, Burma	Island
3.2.6.5	NHM	6'50" N, 101'20"E, Pattani, Siam	
4.438	LKCNHM	6'35"N, 99'40E, Waw, Telok, Pulau Terutao, Thailand	Island
4.448	LKCNHM	8'06"N 98'52"E Ban Nong Kok, Krabi, Thai	
4.45	LKCNHM	8'06"N 98'52"E Ban Nong Kok, Krabi, Thai	
4.455	LKCNHM	7'56"N 98'35"E, Yao Yai, Ko, Phangnga, Thailand	Island
4.46	LKCNHM	5'27"N 100'12"E, Bahang, Telok, Pulau Pinang, W Malaysia	Island
4.463	LKCNHM	5'27"N 100'12"E, Bahang, Telok, Pulau Pinang, W Malaysia	Island
4.465	LKCNHM	6'21"N 101'50"E, Ban Nara, Pattani, Thailand	
4.466	LKCNHM	6'21"N 101'50"E, Ban Nara, Pattani, Thailand	
4.469	LKCNHM	6'21"N 101'50"E, Ban Nara, Pattani, Thailand	

4.47	LKCNHM	6'21"N 101'50"E, Ban Nara, Pattani, Thailand	
4.477	LKCNHM	6'39"N, 100'11"E, Pelarit, Malay, Peris	
4.478	LKCNHM	6'39"N, 100'11"E, Pelarit, Malay, Peris	
4.479	LKCNHM	4'53"N 100'45"E, Tea Garden, Larut Hills, West Malay, Perak	
4.48	LKCNHM	8'06"N 98'52"E Ban Nong Kok, Krabi, Thai	
4.481	LKCNHM	4'19"N, 100'34"E, Tanjong Hantu, Perak, Dinding, Malay	
4.482	LKCNHM	3'44"N 101'14"E, Changkat Mentri, Sungei Bernam, Perka, W Malay	
4.485	LKCNHM	4'45"N 100'45"E, Gantang, Bukit, Perak, W Malay	
4.487	LKCNHM	4'59"N 103'07"E, Bukit Jong, W Malay, Trengganau	
4.488	LKCNHM	4'59"N 103'07"E, Bukit Jong, W Malay, Trengganau	
4.49	LKCNHM	4'01"N 102'18"E, Kuala Tembeling, Pahanag, W Malay	
4.495	LKCNHM	3'40"N 101'45' E, Semangko Pass, Selangor, W Malay	
4.498	LKCNHM	3'14"N 101'20"E, Bukit Chereka Klang, Jeram, Selangor, W malaysia	
4.5	LKCNHM	3'19"N 101'46"E, Genting Bidai, Selangor, W Malay	
4.501	LKCNHM	2'50"N 102'00"E, Bukit Tangga, Negeri Sembilan, W Malay	
4.503	LKCNHM	2'24"N 101'52"E, Keramat Tanjung Tuan, Negeri Sembilan	
4.507	LKCNHM	2'17"N 102'15"E, Nylas, W Malasia, Malaca	
4.509	LKCNHM	2'17"N 102'15"E, Nylas, W Malasia, Malaca	
4.511	LKCNHM	1'25N, 104'05"E, Si Karang, Johor, W Malay	
4.514	LKCNHM	1'31"N 103'35" E, Tebrau, Johor, W Malay	
4.522	LKCNHM	11'49"N 99'45"E, Prachuap Khiri Khan, Thailand	
4.525	LKCNHM	10'28"N, 98' 55"E, Ban Tha San, Chumphon, Thailand	
4.527	LKCNHM	5'54"N 102'45"E, Perhentian Besar Island, Pulau, Trengganau, W Malaysia	Island
4.529	LKCNHM	5'54"N 102'45"E, Perhentian Besar Island, Pulau, Trengganau, W Malaysia	Island

55.1534	NHM	3'40"N, 101'45"E, Semangko Pass, Selangorpahang Boundary, Malay
55.1535	NHM	3'18"N, 101'49" E, Genting Bidai, Selangor, Malay
55.154	NHM	4'19"N, 100'34"E, Tanjong Hantu, Perak, Dinding, Malay
55.1542	NHM	6'39"N, 100'11"E, Pelarit, Perlis, N Malay Pennisula., Malay
71.722	NHM	4'29"N, 100'55"E, Changkat Cheko, Parit, Malay
71.734	NHM	5'02"N, 100'39"E, Bukit Merah, Perak, Malay
71.735	NHM	5'02"N, 100'39"E, Bukit Merah, Perak, Malay, 1800ft
71.749	NHM	3'51"30"'N, 102'11"25"'E, Mt. Benom, Pahang, Malay, 1800ft

† NHM, the Natural History Museum (London, UK); NMNH, the National Museum of Natural History (Washington DC, USA); LKCNHM, the Lee Kong Chian Natural History Museum (Singapore).

435

Appendix 2. Landmarks used in this study.

Landmark	Definition
1	Prosthion: antero-inferior point on projection of pre-maxilla between central incisors
2	Leftside zygo-temp inferior: infero-lateral point of zygomaticotemporal suture on lateral face of zygomatic arch
3	Rightside zygo-temp inferior: infero-lateral point of zygomaticotemporal suture on lateral face of zygomatic arch
4	Lambda: junction of sagittal and lamboid sutures
5	Bregma: junction of coronal and sagittal sutures
6	Leftside frontomalare temporale: where frontozygomatic suture crosses lateral edge of zygoma
7	Rightside frontomalare temporale: where frontozygomatic suture crosses lateral edge of zygoma
8	Leftside frontomalare orbitale: where frontozygomatic suture crosses inner orbital rim
9	Rightside frontomalare orbitale: where frontozygomatic suture crosses inner orbital rim
10	Leftside supraorbital notch
11	Rightside supraorbital notch
12	Leftside meeting point of frontal, nasal, and lacrimal
13	Rightside meeting point of frontal, nasal, and lacrimal
14	Leftside zygo-max superior: antero-superior point of zygomaticomaxillary suture taken at orbit rim
15	Rightside zygo-max superior: antero-superior point of zygomaticomaxillary suture taken at orbit rim
16	Nasion: midline point on fronto-nasal suture
17	Rhinion: most anterior midline point on nasals
18	Rightside most lateral meeting point of mastoid part of temporal bone and occipital
19	Leftside most lateral meeting point of mastoid part of temporal bone and occipital
20	Rightside meeting point of mastoid, occipital and petrosal
21	Leftside meeting point of mastoid, occipital and petrosal
22	Rightside meeting point between sphenoid, occipital and petrosal

23	Leftside meeting point between sphenoid, occipital and petrosal
24	Rightside most medial point of medial pterygoid fossa
25	Leftside most medial point of medial pterygoid fossa
26	Rightside meeting point of petrous part of temporal bone, alisphenoid and base of zygomatic process of temporal bone
27	Leftside meeting point of petrous part of temporal bone, alisphenoid and base of zygomatic process of temporal bone
28	Rightside zygo-max inferior: antero-inferior point of zygomaticomaxillary suture
29	Leftside zygo-max inferior: antero-inferior point of zygomaticomaxillary suture
30	Rightside M3 distal midpoint projected (laterally) onto alveolar margin
31	Leftside M3 distal midpoint projected (laterally) onto alveolar margin
32	Tip of posterior nasal spine
33	Rightside anterior-most point of canine alveolus
34	Leftside anterior-most point of canine alveolus
35	Leftside most posterior tip of occlusal surface of M3
36	Leftside most posterior tip of occlusal surface of M2
37	Leftside most posterior tip of occlusal surface of M1
38	Leftside most posterior tip of occlusal surface of P4
39	Leftside most posterior tip of occlusal surface of P3
40	Leftside most anterior tip of occlusal surface of P3
41	Rightside most posterior tip of occlusal surface of M3
42	Rightside most posterior tip of occlusal surface of M2
43	Rightside most posterior tip of occlusal surface of M1
44	Rightside most posterior tip of occlusal surface of P4
45	Rightside most posterior tip of occlusal surface of P3
46	Rightside most anterior tip of occlusal surface of P3

47	Rightside condylion
48	Leftside condylion
49	Rightside most medial point of mandible condyle
50	Leftside most medial point of mandible condyle
51	Rightside most inferior point of mandibular notch
52	Leftside most inferior point of mandibular notch
53	Rightside Coronion
54	Leftside Coronion
55	Rightside most posterior point on the ascending ramus in line with the alveolus
56	Leftside most anterior point on the ascending ramus in line with the alveolus
57	Rightside Gonion
58	Leftside Gonion
59	Rightside most anterior insertion of digastric
60	Leftside most anterior insertion of digastric
61	Gnathion
62	Rightside most anterior point on the ascending ramus in line with the alveolus
63	Leftside most anterior point on the ascending ramus in line with the alveolus
64	Ligunal-side most superior point of mandibular symphysis
65	Rightside most posterior point of canine alveolus
66	Leftside most posterior point of canine alveolus
67	Symphysion

436

437

Appendix 3. Model selection table.

Intercept	Size	Latitude	Region (south vs. north of IOK)	Annual mean temperature	Annual precipitation	ΔAIC
PC4						
0.12			0.34			0.00
0.12		0.14	0.45			1.36
0.12	-0.04		0.34			1.85
0.11			0.33	0.06		1.88
0.12			0.34		-0.04	1.89
0.12	-0.04	0.14	0.45			3.24
0.11		0.14	0.44	0.04		3.31
0.12		0.14	0.45		-0.02	3.33
0.11	-0.04		0.33	0.06		3.71
0.12	-0.03		0.34		-0.03	3.80
0.11			0.33	0.05	-0.03	3.82
PC8						
0.02	-0.24	-0.54	-0.54			0.00
0.02		-0.52	-0.53			1.30
0.00	-0.25	-0.56	-0.57	0.09		1.83
0.01	-0.23	-0.56	-0.56		-0.05	1.91
0.01	-0.23					2.47
0.01		-0.56	-0.58		-0.13	2.64
0.01						3.10
0.01		-0.53	-0.55	0.06		3.24
0.01	-0.24	-0.12				3.79
0.01	-0.22		-0.12			3.80
0.00	-0.24	-0.56	-0.57	0.08	-0.03	3.80
0.02			-0.13			4.36
0.01	-0.24				0.05	4.38
0.01	-0.23			-0.04		4.43
0.01		-0.10				4.61
0.01		-0.56	-0.58	0.01	-0.13	4.64

Models that have ΔAIC < 5 are shown.

438

Figure 1

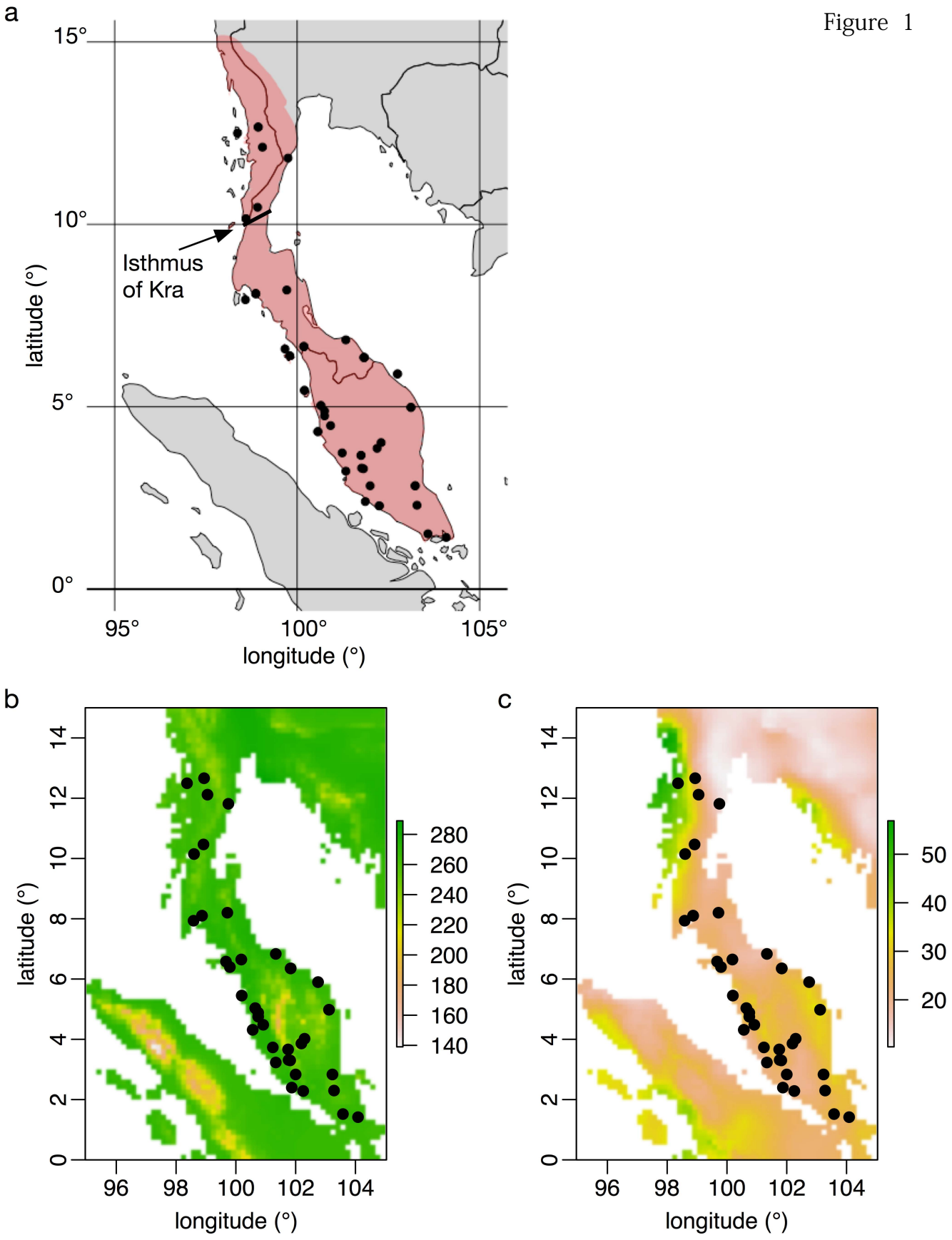
a
15°
10°
5°
0°
latitude (°)
Isthmus
of Kra
95°
100°
105°
longitude (°)
b
latitude (°)
0
2
4
6
8
10
12
14
96
98
100
102
104
longitude (°)
280
260
240
220
200
180
160
140
c
latitude (°)
longitude (°)
50
40
30
20

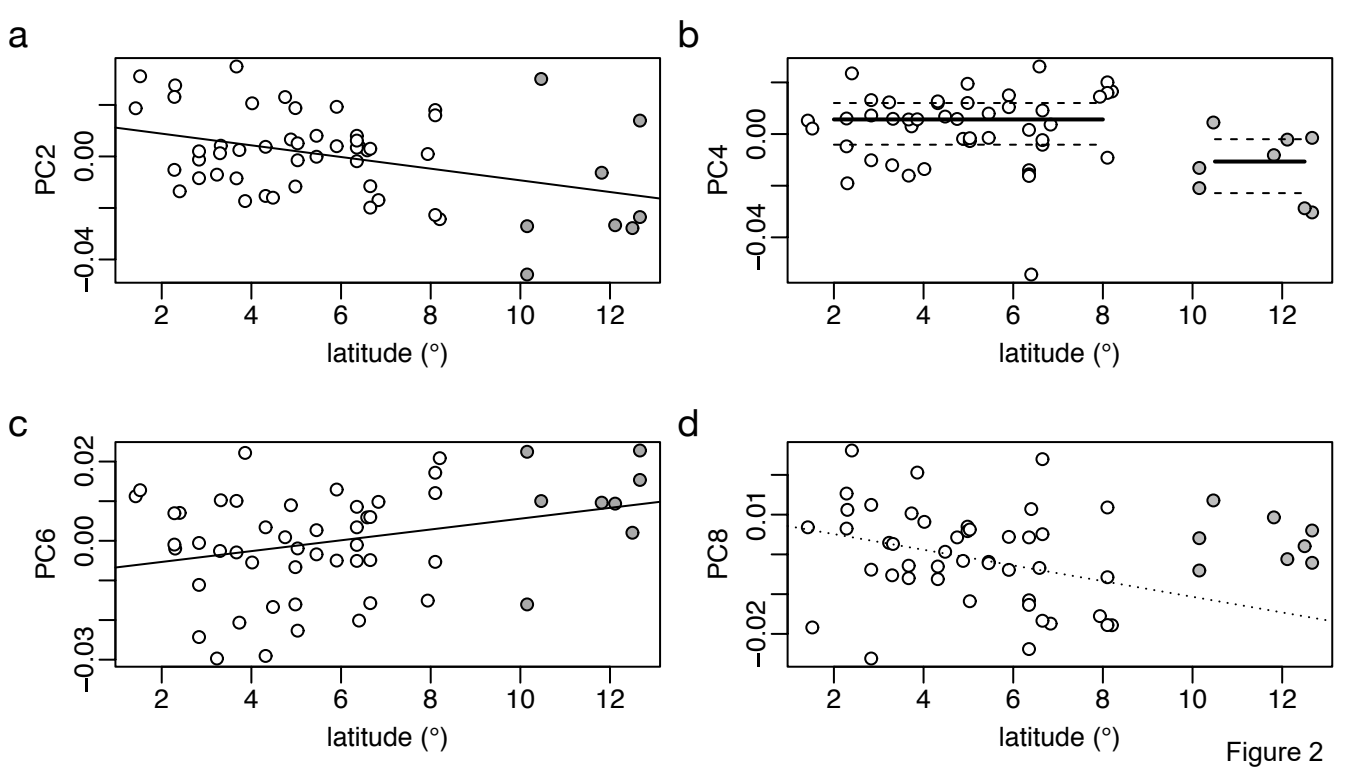
a
PC2
0.00
−0.04
2
4
6
8
10
12
latitude (°)
b
PC4
0.00
−0.04
2
4
6
8
10
12
latitude (°)
c
PC6
0.02
0.00
−0.03
2
4
6
8
10
12
latitude (°)
d
PC8
0.01
−0.02
2
4
6
8
10
12
latitude (°)

Figure 2

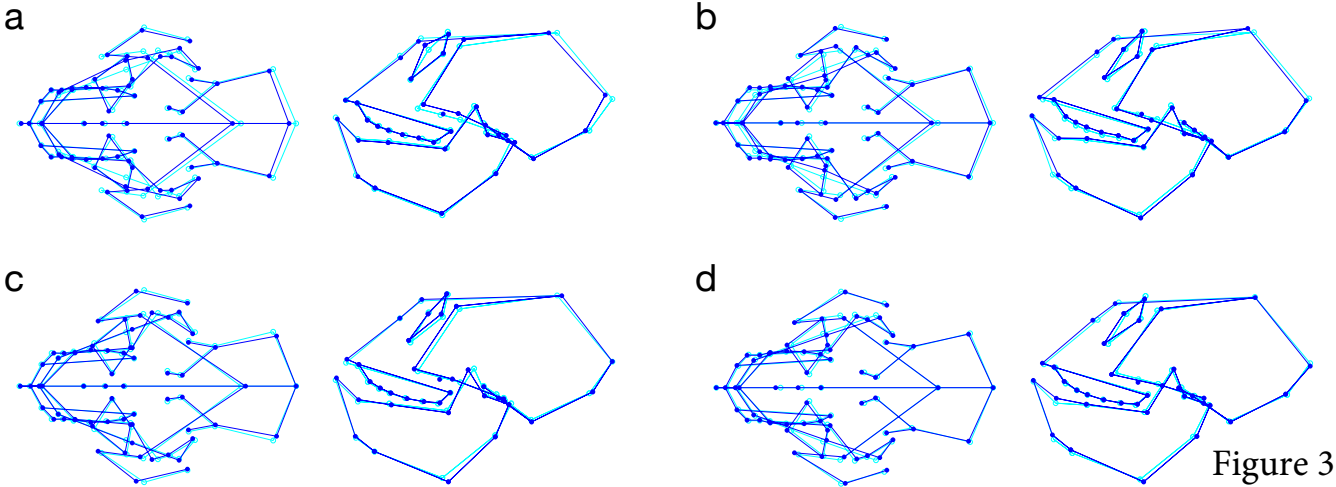

Figure 3

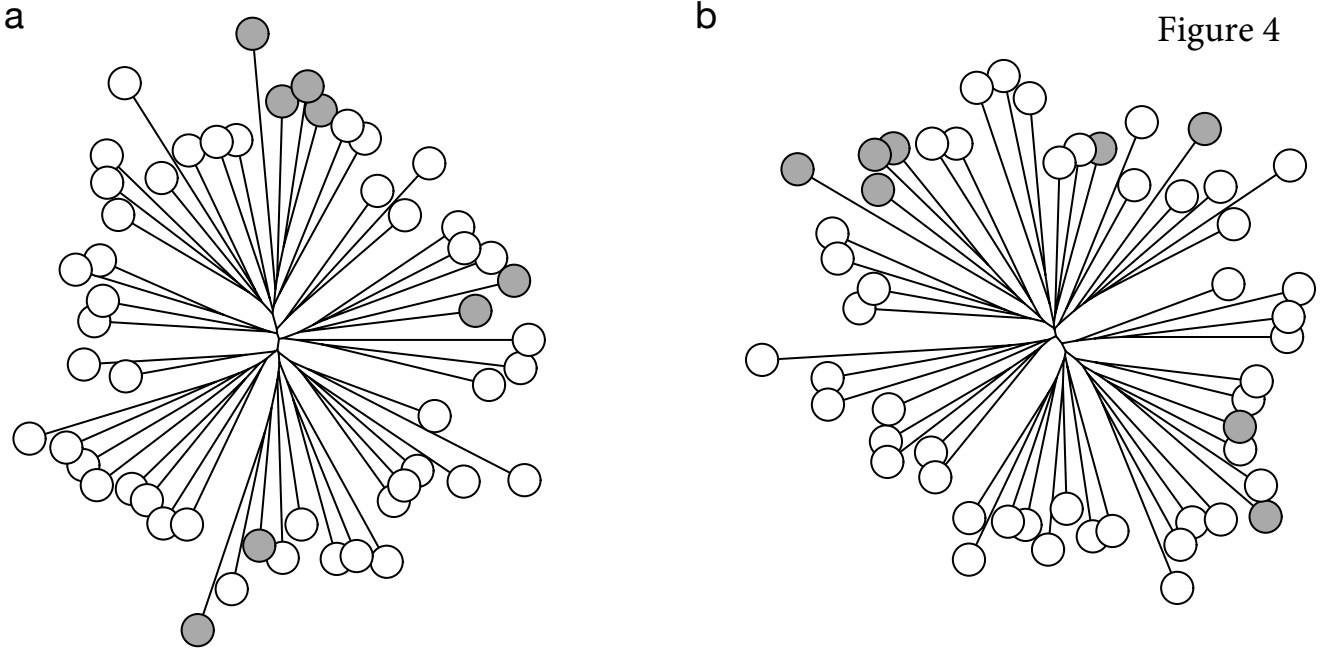

Figure 4